Collective-effects-enhanced multiqubit information engines

Noufal Jaseem [*] and Victor Mukherjee

Department of Physical Sciences, Indian Institute of Science Education and Research Berhampur, Berhampur 760010, India

We study a quantum information engine (QIE) modeled by a multiqubit working medium (WM) collectively coupled to a single thermal bath. We show that one can harness the collective effects to significantly enhance the performance of the QIE, as compared to equivalent engines lacking collective effects. We use one bit of information about the WM magnetization to extract work from the thermal bath. We analyze the work output, noise-to-signal ratio, and thermodynamic uncertainty relation (TUR), and contrast these performance metrics of a collective QIE with that of an engine whose WM qubits are coupled independently to a thermal bath. We show that in the limit of high temperatures of the thermal bath, a collective QIE always outperforms its independent counterpart. In contrast to quantum heat engines, where collective enhancement in specific heat plays a direct role in improving the performance of the engines, here the collective advantage stems from higher occupation probabilities for the higher-energy levels of the positive magnetization states, as compared to the independent case. Furthermore, we show that in the limit of high temperatures, the TUR for both the collective as well as the independent QIEs violate the standard heat engine TUR bound of 2.

I. INTRODUCTION

The relationship between information theory and thermodynamics has been a topic of intense interest in the research community during the last few decades [1], with information engines, i.e., engines which use information to extract useful work, playing a significant role in this regard [2–4]. The concept of Maxwell's demon [5], first proposed by James Clerk Maxwell in 1867, was one of the earliest works suggesting the possibility of using information to extract work from a single heat bath in classical systems. Subsequently, the idea of using information and measurements to extract work was extended to the quantum regime [1,2,4,6–17], and also realized experimentally in recent years [18,19].

One of the major aims of the field of quantum thermodynamics is to study the effects of quantum physics on the operation of quantum machines [20–23]. For example, quantum coherence has been shown to improve the power output of quantum heat engines [24], while squeezed thermal reservoirs have been used to significantly enhance the efficiencies of such engines [25–27]; nonadiabatic excitations in quantum critical systems driven out of equilibrium have been shown to aid in the charging of quantum batteries [28], and entanglement may help in extracting work from such batteries [29]. Quantum features have been used to design quantum information engines (QIEs) as well. For example, a bosonic quantum Szilard engine has been shown to outperform its fermionic counterpart [2]. Reference [13] showcases the use of quantum coherence to extract nontrivial work from the process of unselective measurements, akin to information erasure. This stands in contrast to the Landauer principle, which imposes a thermodynamic work cost for both classical and quantum erasure.

In recent years, collective effects in many-body quantum technologies comprising indistinguishable particles collectively coupled to thermal baths have received significant attention from the research community [30–35]. For example, collective effects have been used to perform high-precision quantum thermometry [32] and to obtain enhanced work output [30–32], efficiency [36], and reliability [34] in quantum thermal machines. In this paper, we propose a collective effects enhanced many-body QIE, modeled by a working medium (WM) of n noninteracting indistinguishable spin-1/2's, collectively coupled to a single heat bath. Information about the magnetization direction of the WM allows us to extract work. Our analysis shows that in comparison to an equivalent QIE modeled by n noninteracting spin-1/2's independently coupled to heat baths, the collective effects may result in significantly enhanced work output, a low noise-to-signal ratio, and low thermodynamic uncertainty ($\mathcal{Q}$). The collective advantage originates from higher occupation probabilities for the higher-energy levels of the positive magnetization states compared to the independent case.

The paper is organized as follows. In Sec. II, we discuss the model of the many-body QIE, its operation, and the process of work extraction, in detail. The different performance metrics of the QIE are studied, and compared with their independent QIE counterparts, in Sec. III. Finally, we summarize our results in Sec. IV.

II. MANY-BODY INFORMATION ENGINE

A. Information engine

We consider a working medium (WM) consisting of n spin-1/2 systems. One can model a three-stroke information engine as follows (see Fig. 1):

Stroke 1: In the first energizing stroke, the WM is coupled to a thermal bath at an inverse temperature β. The WM

---

*Corresponding author: noufaljp@iiserbpr.ac.in
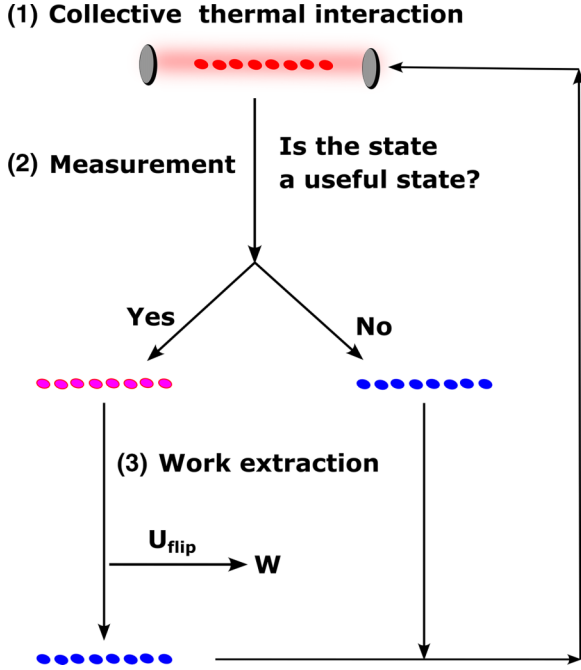
(1) Collective thermal interaction

FIG. 1. A schematic representation of an information engine comprising n qubits, highlighting the three strokes of the cycle.

undergoes a nonunitary evolution, wherein energy flows from the bath to the system, resulting in the WM reaching a steady-state $\rho^{\rm ss}$ at long times.

Stroke 2: In the second stroke, the WM is decoupled from the bath, and the direction of the magnetization m of the WM, or equivalently, the sign of m, is measured. A positive magnetization implies the WM has nonzero ergotropy, i.e., the maximum work that can be extracted via suitable unitary operations [37]. A part of the ergotropy can be extracted by applying a global unitary $U_{\rm flip}$ to flip all the qubits of the WM.

Stroke 3: Following the result of the measurement in stroke 2, we apply a global unitary $U_{\rm flip}$ to flip all the qubits of the WM for $m > 0$, thereby changing the sign of m, and extracting work in the process. On the other hand, a negative m is detrimental to work extraction under the above unitary $U_{\rm flip}$. Consequently, no unitary is applied in the case of $m \leqslant 0$.

Finally, we couple the WM with the Markovian bath introduced in stroke 1, and repeat all the steps mentioned above, thereby giving rise to a cyclic information engine.

B. Model and dynamics

In this section, we discuss in detail the dynamics involved in stroke 1 of the information engine, introduced above. To this end, we consider a WM composed of multiple noninteracting qubits with a bare Hamiltonian given by $H = \hbar\omega\mathcal{J}_z$, where we define the collective angular momentum operators as $\mathcal{J}_i := \frac{1}{2}\sum_{k=1}^{n}\sigma_i^k$. Here, the Pauli matrix σ_i^k is the spin operator along the i axis ($i = x, y, z$), acting on the kth spin. The spins are collectively coupled to a thermal bath during the nonunitary stroke 1 through the system-bath interaction Hamiltonian $H_{\rm int} = \gamma \mathcal{J}_x \otimes \mathcal{B}$. Here, γ denotes the coupling strength, while $\mathcal{B}$ is an operator acting on the thermal bath. As shown in Refs. [30,32,38], such a collective system-bath

interaction may generate quantum coherence in the steady-state density matrix $\rho_{\rm col}^{\rm ss}$ of the WM, characterized by the presence of off-diagonal elements in the WM density matrix in the local spin basis. The dynamics of the WM is described by the master equation [30,32,38]

$$\frac{d\rho}{dt} = -\frac{i}{\hbar}[H, \rho] + \Gamma(\omega)\mathcal{D}(\mathcal{J}^+)\rho + \Gamma(-\omega)\mathcal{D}(\mathcal{J}^-)\rho, \quad (1)$$

where $\mathcal{D}[O]\rho = (2O^\dagger\rho O - OO^\dagger\rho - \rho OO^\dagger)/2$, the collective ladder operators of the spin system are given by $\mathcal{J}^\pm := \mathcal{J}_x \pm i\mathcal{J}_y$, and $\Gamma(\omega)$ is the spectral function of the bath at frequency ω. The spectral functions $\Gamma(\omega)$ and $\Gamma(-\omega)$ are related to each other via the Kubo-Martin-Schwinger condition $\Gamma(-\omega) = \exp(-\beta\hbar\omega)\Gamma(\omega)$ [39]. The steady-state $\rho_{\rm col}^{\rm ss}$ can be expressed in the collective basis $|j, m\rangle_i$ of the common eigenvectors of $\mathcal{J}_z$ and $\mathcal{J}^2 = \mathcal{J}_x^2 + \mathcal{J}_y^2 + \mathcal{J}_z^2$ as [38]

$$\rho_{\rm col}^{\rm ss}(\beta, \omega) = \sum_{j=j_0}^{n/2}\sum_{i=1}^{l_j} P_{j,i}\, \rho_{j,i}^{\rm th}(\beta, \omega),$$

$$\rho_{j,i}^{\rm th}(\beta, \omega) = \frac{1}{Z_j}\sum_{m=-j}^{j} e^{-\beta m\hbar\omega}|j, m\rangle_{ii}\langle j, m|. \quad (2)$$

Here, $Z_j = \sum_{m=-j}^{j} e^{-\beta m\hbar\omega}$ is the partition function of the angular momentum subspace j, $-j \leqslant m \leqslant j$, $j \in [j_0; n/2]$, and $j_0 = 1/2$ for odd n and $j_0 = 0$ for even n. The index $i \in [1; l_j]$, where l_j is the multiplicity of the eigenspaces associated with the eigenvalue j of the operator $\mathcal{J}^2$ [40]. The initial state ρ_0 of the WM determines the probability $P_{j,i}$ through the relation $P_{j,i} = \sum_{m=-j}^{j} {}_i\langle j, m|\rho_0|j, m\rangle_i$.

Previous studies have shown that an initial state prepared in the $j = n/2$ subspace is the most favorable for obtaining collective advantage in quantum thermal machines [30,32,34]. Consequently, here we restrict ourselves to the $j = n/2$ subspace, such that $l_{j=n/2} = 1$, $P_{j=n/2} = 1$, and the corresponding steady state is given by [23,32]

$$\rho_{\rm col}^{\rm ss}(\beta, \omega) = \frac{1}{Z_{n/2}}\sum_{m=-n/2}^{n/2} e^{-\beta m\hbar\omega}\left|\frac{n}{2}, m\right\rangle\left\langle\frac{n}{2}, m\right|. \quad (3)$$

We note that in contrast to the setup introduced above, one can consider an independent WM-bath coupling, described by an interaction Hamiltonian of the form $H_{\rm int} = \frac{\gamma}{2}\sum_{k=1}^{n}\sigma_x^k \otimes \mathcal{B}_k$, where $\mathcal{B}_k$ denotes an operator acting on the bath coupled to the kth spin. In the latter scenario, the steady state reached at the end of the nonunitary thermal interaction stroke is a direct product state of the form [23,30,32,38,39]

$$\rho_{\rm ind}^{\rm ss}(\beta, \omega) = \otimes_{k=1}^{n}\rho_k^{\rm ss}(\beta, \omega), \quad (4)$$

where $\rho_k^{\rm ss}(\beta, \omega) = \frac{\exp(-\beta\hbar\omega\sigma_z^k/2)}{{\rm Tr}[\exp(-\beta\hbar\omega\sigma_z^k/2)]}$ is the steady-state density matrix corresponding to the kth spin.

III. STATISTICS OF THE OUTPUT WORK

The unitary operation $U_{\rm flip}$ considered in the second stroke introduced in Sec. II A acts only the states $|n/2, m\rangle$ with $m > 0$; a part of the ergotropy of such states is extracted in the form of output work, while those states are transformed to $|n/2, -m\rangle$ at the end of this stroke. For the independent bath

coupling as well, a state $|m\rangle$ with $m > 0$ denotes the presence of nonzero ergotropy, which can be used to perform useful work through unitary transformation to the state $|-m\rangle$. We take the sign of energy outflow from the WM as positive and the inflow as negative. If $w_m = 2m\hbar\omega$ is the amount of work extracted from the state $|n/2, m\rangle$ or from $|m\rangle$ with probability p_m^α (α = col., ind.), then the average work takes the form

$$\langle W_\alpha \rangle = \sum_{m \geqslant 0} w_m p_m^\alpha, \tag{5}$$

and its variance, $\text{var}(W_\alpha) = \langle W_\alpha^2 \rangle - \langle W_\alpha \rangle^2$, is given by

$$\text{var}(W_\alpha) = \sum_{m \geqslant 0} w_m^2 p_m^\alpha - \langle W_\alpha \rangle^2. \tag{6}$$

In Eqs. (5) and (6), $m = 0, 1, 2, \ldots, n/2$ for even n, while $m = 1/2, 3/2, 5/2, \ldots, n/2$ for odd n. For the collective engine, the probability is given by [see Eq. (3)]

$$p_m^{\text{col}} = \frac{e^{-\beta m\hbar\omega}}{Z_{n/2}}, \tag{7}$$

while in the case of the independent engine, we have [see Eq. (4)]

$$p_m^{\text{ind}} = {}^nC_{n/2-m} \frac{e^{-\beta m\hbar\omega}}{Z_{\text{ind}}}, \qquad {}^rC_s \equiv \frac{r!}{(r-s)!s!}. \tag{8}$$

Here, $Z_{\text{ind}} = (e^{-\beta\omega/2} + e^{\beta\omega/2})^n$ is the partition function corresponding to the thermal state of the independent engine's WM. The factor ${}^nC_{n/2-m}$ in Eq. (8) denotes the number of combinations of spin arrangements that give rise to a magnetization m.

A. Information engine in the high-temperature limit

In the limit $\beta = \frac{1}{k_B T} \to 0$, all the basis states will have an equal probability of being occupied, and hence from Eq. (5), we get the collective work output as (see Appendix),

$$\lim_{\beta \to 0} \langle W_{\text{col}} \rangle = \lim_{\beta \to 0} \sum_{m \geqslant 0} w_m p_m^{\text{col}} = \frac{\hbar\omega}{n+1} \sum_{r=0}^{r_{\max}} (n - 2r). \tag{9}$$

Here, $p_m^{\text{col}}(\beta \to 0) = 1/(n+1)$, $w_m = 2\hbar\omega m = \hbar\omega(n - 2r)$ with $r = n/2 - m$, $r_{\max} = n/2$ for even n, and $r_{\max} = (n-1)/2$ for odd n. The above equation simplifies to $\langle W_{\text{col}} \rangle = (n+1)\hbar\omega/4$ for odd n, and to $\langle W_{\text{col}} \rangle = \frac{n(n+2)}{4(n+1)}\hbar\omega$ for even n, which, in the limit of large n, can be approximated to $n\hbar\omega/4$. Similarly, the work output for the independent case can be obtained as

$$\lim_{\beta \to 0} \langle W_{\text{ind}} \rangle = \lim_{\beta \to 0} \sum_{m \geqslant 0} p_m^{\text{ind}} w_m = \frac{\hbar\omega}{2^n} \sum_{r=0}^{r_{\max}} {}^nC_r (n - 2r), \tag{10}$$

where $p_m^{\text{ind}}(\beta \to 0) = {}^nC_r/2^n$ and $w_m = \hbar\omega(n - 2r)$. The above equation readily simplifies to $\langle W_{\text{ind}} \rangle = 2^{-(n+1)} \, {}^nC_{\frac{n+1}{2}} (n+1)\hbar\omega$ for odd n and $\langle W_{\text{ind}} \rangle = \frac{1}{2^{n+1}} {}^nC_{\frac{n}{2}} n\hbar\omega$ for even n. By identifying the Catalan number $\mathbb{C}_r = \frac{1}{r+1} \, {}^{2r}C_r$ [41,42] which approximates to $4^r/(r\sqrt{r\pi})$ in the large r limit, we get $\langle W_{\text{ind}} \rangle \approx \sqrt{\frac{n}{2\pi}}\hbar\omega$ for both odd and even n. From the above, the ratio of the work output of the collective to the
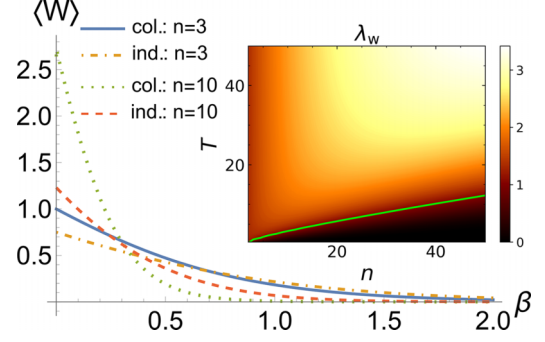

FIG. 2. The average work outputs $\langle W_{\text{col}} \rangle$ and $\langle W_{\text{ind}} \rangle$ are plotted as functions of β for $n = 3$ and $n = 10$. In the inset, we present the variation of the ratio $\lambda_{\text{w}} = \langle W_{\text{col}} \rangle / \langle W_{\text{ind}} \rangle$ with respect to n and $T = 1/\beta$. The green contour line represents $\lambda_{\text{w}} = 1$. The values of $\hbar$, k_B, and ω are set to 1.

independent case can be calculated to be

$$\lambda_{\text{w}} = \frac{\langle W_{\text{col}} \rangle}{\langle W_{\text{ind}} \rangle} \approx \frac{\sqrt{2\pi n}}{4}, \tag{11}$$

for large n values (see Fig. 2). Therefore we get a quadratic increase in the output work for the collective engine over the independent one, as also shown in Fig. 3.

We note that as discussed in Refs. [32,34], in the case of a collective quantum heat engine, the improvement in its performance is a direct consequence of the collective enhancement in the specific heat, which depends on the populations and the energies of all the magnetization m states of the WM. In contrast, in the QIE introduced here, only the $m > 0$ states contribute to work extraction (see Sec. II A); in this case, the collective advantage stems from higher occupation probabilities p_m^{col} for large $m > 0$ (see the inset of Fig. 3), as
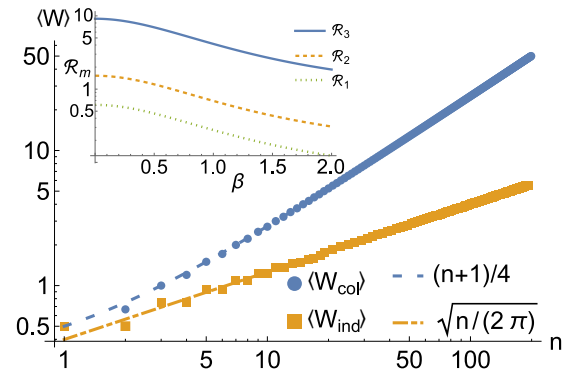

FIG. 3. The work output of the collective and independent engines given in Eqs. (9) and (10) are plotted as functions of the number of qubits n, for $\beta \to 0$. The dashed and dotted-dashed lines represent the work output obtained in the large n limit. Inset: The figure depicts the ratios of the occupation probabilities, denoted as $\mathcal{R}_m \equiv p_m^{\text{col}}/p_m^{\text{ind}}$, for $m = 1, 2, 3$ against the inverse temperature β for a system comprising $n = 6$ spin particles. The plot illustrates that the collective occupation probabilities for the higher-energy levels ($m = 2, 3$) remain larger than the corresponding independent probabilities over a range of high temperatures. The values of $\hbar$, k_B, and ω are set to 1.
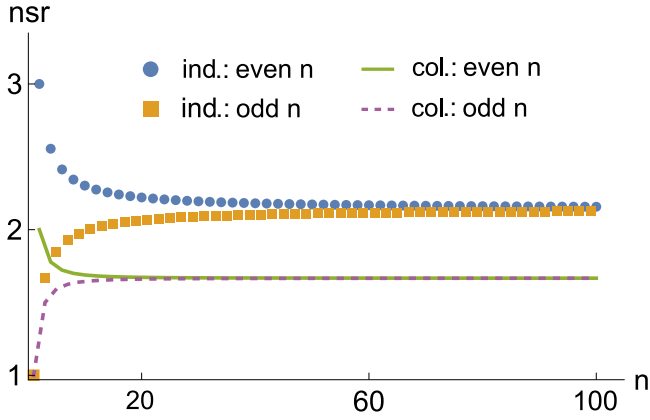
FIG. 4. The plot shows the noise-to-signal ratios for the collective (nsr_col) and the independent (nsr_ind) cases as functions of the number of qubits n, for $\beta \to 0$. The values of $\hbar$, k_B, and ω are set to 1.

compared to p_m^ind for an independent QIE, which we discuss below. In the limit of high temperatures ($\beta \to 0$), the partition functions for the collective and independent cases are given by $Z_\text{col} = n + 1$ and $Z_\text{ind} = 2^n$. With the working medium state constrained to the $j = n/2$ subspace, there is a unique eigenstate corresponding to $|n/2, m\rangle$, while for the independent case, there are $^nC_{n/2-m}$ degenerate eigenstates $|m\rangle$; the degeneracy $^nC_{n/2-m}$ increases with decreasing $|m|$. Consequently, p_m^ind surpasses p_m^col for smaller values of $|m|$. A similar analysis for finite temperatures shows that collective advantages persist for $n\beta \ll 2/(\hbar\omega)$, as shown by the ratio $\mathcal{R}_m = p_m^\text{col}/p_m^\text{ind}$ for large $m > 0$ [see Eqs. (7) and (8) and Fig. 3].

Noise-to-signal ratio and TUR

The reliability of an engine can be quantified through the noise-to-signal ratio $\text{nsr} = \text{var}(W)/\langle W \rangle^2$. One can calculate the variance of work for the collective and independent cases for $\beta \to 0$ as [see Eqs. (6)–(8)]

$$\text{var}(W_\text{col}) = \frac{\hbar^2\omega^2}{n+1} \sum_{r=0}^{r_\text{max}} (n - 2r)^2$$
$$- \left(\frac{\hbar\omega}{n+1} \sum_{r=0}^{r_\text{max}} (n - 2r) \right)^2, \qquad (12)$$

and

$$\text{var}(W_\text{ind}) = \frac{\hbar^2\omega^2}{2^n} \sum_{r=0}^{r_\text{max}} {}^nC_r(n - 2r)^2$$
$$- \left(\frac{\hbar\omega}{2^n} \sum_{r=0}^{r_\text{max}} {}^nC_r(n - 2r) \right)^2. \qquad (13)$$

As shown in Fig. 4, for small values of n, odd values yield a lower nsr compared to even values, both for collective as well as independent engines. However, as n increases, the nsr's for both even and odd values converge asymptotically, with the asymptotic value in the collective case being smaller than that in the independent case, demonstrating a collective advantage in engine performance.

As discussed in Ref. [43], a low nsr can be accompanied by a large entropy production Σ in heat engines, which in turn, can be expected to reduce the efficiencies of such engines. A trade-off between nsr and Σ can be quantified using the thermodynamic uncertainty, expressed as $\mathcal{Q} \equiv \text{nsr}\,\Sigma/k_B$, which is generally lower bounded by the inequality $\mathcal{Q} \geqslant 2$ in the case of classical [44–46] and incoherent quantum [47–49] heat engines. Recently, violations of this inequality have been observed for quantum-coherent and quantum-entangled systems [34,47,50–54]. The behavior of $\mathcal{Q}$ in the case of information engines can be an interesting question as well [55]. In the case of the collective and independent QIEs considered here, analogous to Szilard engines [2], the minimum entropy production arising due to memory erasure is given by $\Delta S_\text{era}^\text{min} = k_B \ln 2$. Consequently, in contrast to what is expected for incoherent quantum heat engines [47–49], the minimum thermodynamic uncertainty $\mathcal{Q}_\text{min} = \ln 2\,\text{nsr}$, which in the limit of large n, is less than the standard limit of $\mathcal{Q} = 2$ discussed above (see Fig. 4). The above result of $\mathcal{Q} < 2$ for large n raises important questions regarding the validity of the standard thermodynamic uncertainty bound in the case of information engines. However, a detailed study of thermodynamic uncertainty bounds for generic QIEs is beyond the scope of the present work. Furthermore, we note that collective WM-bath coupling leads to the emergence of nontrivial steady states, signified by nonzero off-diagonal elements in $\rho_\text{col}^\text{ss}$ in the local eigenbasis [see Eq. (3)] [32]. This in turn have been shown to reduce the thermodynamic uncertainty $\mathcal{Q}$ below the standard bound of 2, for quantum heat engines [34].

B. Finite-temperature information engine

We now focus on the finite-temperature regime. The mean and variance of the output work, as well as the nsr, can be evaluated using Eqs. (5) and (6) for arbitrary n and β [see Figs. 2, 5(a), and 6(a)]. Detailed equations for calculating the mean and variance can be found in the Appendix [see Eqs. (A1)–(A8)]. In the limit of large n, the analysis for the collective case can be simplified by replacing the summations in Eqs. (5) and (6) with integrations to get

$$\langle W_\text{col} \rangle = \frac{[\beta\hbar\omega(n - 2r_\text{max}) + 2]\,e^{\beta\hbar\omega r_\text{max}} - n\beta\hbar\omega - 2}{\beta(e^{\beta n\hbar\omega} - 1)}. \quad (14)$$

As expected, Eq. (14) simplifies to $\langle W_\text{col} \rangle \approx n\hbar\omega/4$ in the limit of $\beta \to 0$ (see Sec. III A). Furthermore, as discussed above, the collective advantage manifests itself for high temperatures $n\beta \ll 2/(\hbar\omega)$. In contrast, numerical analysis confirms that independent engines outperform their collective counterparts for low temperatures [see Fig. 5(a)].

We note that in accordance with the second law of thermodynamics, in an information engine operating at a temperature T, the maximum extractable work $\sim k_B T$ (see above). Again, as discussed in Sec. III A, in the limit of large temperatures ($k_B T \gg n\hbar\omega$), $\langle W_\text{col} \rangle \sim n\hbar\omega$ ($\langle W_\text{ind} \rangle \sim \sqrt{n}\hbar\omega$) for the collective (independent) case, which increases with increasing n, until $\langle W_\text{col} \rangle \sim k_B T$ ($\langle W_\text{ind} \rangle \sim k_B T$). Consequently, the optimal system size scales as $n_\text{opt}^\text{(col)} \sim k_B T/\hbar\omega$ [$n_\text{opt}^\text{(ind)} \sim (k_B T/\hbar\omega)^2$] for high temperatures for the collective (independent) case, as also verified by the inset of Fig. 5(a). For $n \gtrsim n_\text{opt}^\text{(col)}$
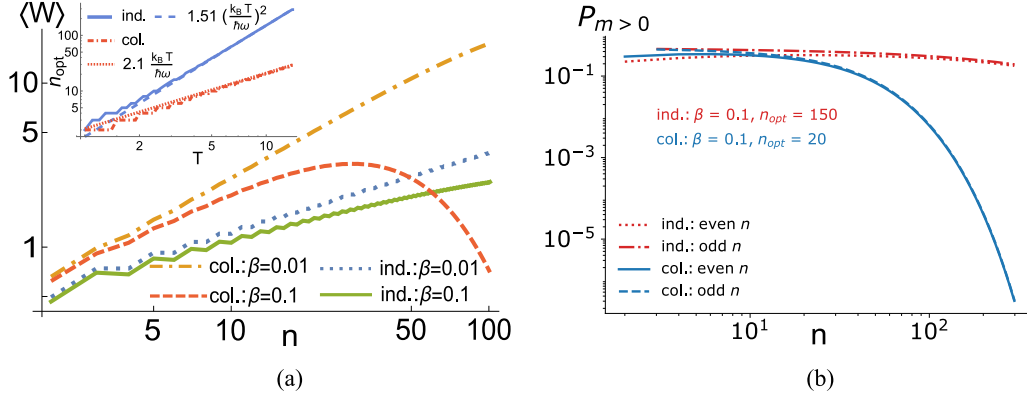
FIG. 5. (a) The work output of the collective and independent engines are plotted as functions of the number of qubits n, for $\beta = 0.01$ and 0.1 [see Eqs. (5), (7), and (8)]. Inset: The optimal qubit number $n_{\text{opt}}^{(\alpha)}$ (α = col., ind.), at which the work output is maximum for a given temperature, is plotted as functions of temperature T. Numerical fitting suggests $n_{\text{opt}}^{(\text{col})} \approx 2.1 k_B T / \hbar\omega$ and $n_{\text{opt}}^{(\text{ind})} \approx 1.51 (k_B T / \hbar\omega)^2$. (b) The graph depicts the probability of obtaining a positive m during the measurement stroke 2, given by $P_{m>0}$, at finite temperature $\beta = 0.1$ for both collective and independent engines. The values of $\hbar$, k_B, and ω are all set to 1 in both figures.

$(n \gtrsim n_{\text{opt}}^{(\text{ind})})$, $\langle W_{\text{col}} \rangle$ ($\langle W_{\text{ind}} \rangle$) decreases with increasing n [see Figs. 5(a) and 7], owing to the small probabilities $P_{m>0}^{\alpha} = \sum_{m>0} p_m^{\alpha}$ [α = col., ind.; see Eqs. (7) and (8)] of getting positive m in the measurement stroke 2 [see Fig. 5(b)].

As shown in Figs. 4 and 6(a), collective effects result in QIEs with low nsr in the high-temperature limit, as compared to their independent counterparts. However, for low temperatures, independent QIEs may be more reliable than the collective ones, as signified by the nsr of collective QIEs surpassing that for independent QIEs, with increasing β, for a fixed finite n [see the Fig. 6(a)].

For a finite-temperature information engine, the entropy change due to the heat exchange between the WM and the heat source is given by $\Delta S_h^{(\alpha)} = -\langle W_\alpha \rangle / T_h$ for α = col., ind., where we have considered the conservation of energy, so that on an average, the work output equals the heat input from the bath. Further, the process of memory erasure results in an increase of entropy of the universe by $\Delta S_{\text{era}} \geqslant k_B \ln 2$. Therefore, the total entropy production is given by $\langle \Sigma_\alpha \rangle = \Delta S_h + \Delta S_{\text{era}}^{\alpha} = -\langle W_\alpha \rangle / T_h + \Delta S_{\text{era}}^{\alpha}$. Utilizing the results for $\langle W_{\text{col}} \rangle$ and $\langle W_{\text{ind}} \rangle$ [cf. Eqs. (A1)–(A4)], it can be shown that the entropy production is always non-negative, as depicted in Fig. 6(b), thereby satisfying the second law of thermodynamics.

Furthermore, the collective effects enhance $\langle W_{\text{col}} \rangle$ at high temperatures for a given n, resulting in reduced entropy production ($\langle \Sigma_{\text{col}} \rangle < \langle \Sigma_{\text{ind}} \rangle$) and reduced thermodynamic uncertainty ($\mathcal{Q}_{\text{col}} < \mathcal{Q}_{\text{ind}}$) for the collective QIE, as compared to its independent counterpart. Assuming the minimal erasure entropy production ΔS_{era} to be equal to $k_B \ln 2$, both the independent and the collective cases violate the standard TUR at high temperatures for a given n (i.e., $\mathcal{Q}_{\text{col}} < \mathcal{Q}_{\text{ind}} < 2$), as shown in Fig. 6(c). $\mathcal{Q}_{\text{col}}$ may surpass $\mathcal{Q}_{\text{ind}}$ at low temperatures, thus again showing the importance of high temperatures for achieving collective advantage in QIEs.

IV. DISCUSSION

In this paper, we have studied a many-body QIE that relies on one bit of information to extract work from a single heat bath. The engine considered here is modeled by a multiqubit system WM interacting collectively with a heat reservoir. The collective effects observed in this system arise from the bath's inability to distinguish between the qubits as they exchange energy, which results in a nontrivial steady state of the WM. Based on the measurement outcome of the net magnetization direction of the steady state, a unitary operation may be performed to extract useful work.
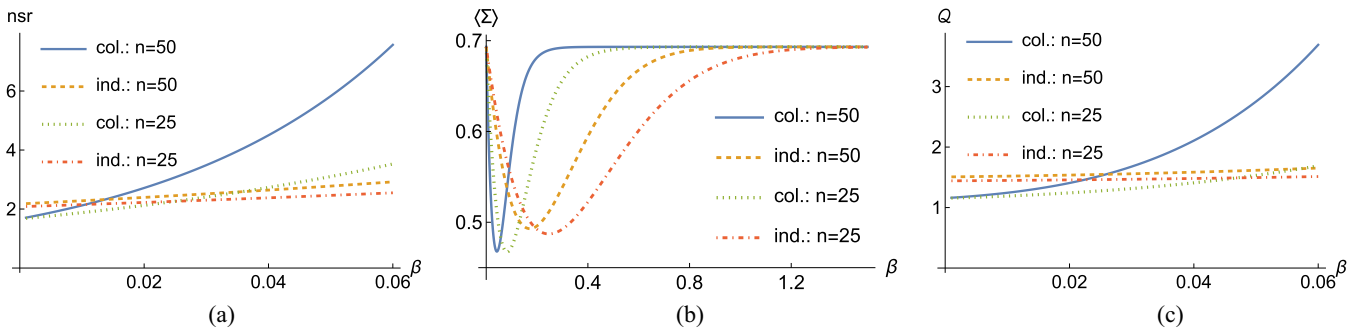

FIG. 6. The plots depict (a) the noise-to-signal ratio nsr, (b) the total average entropy production $\langle \Sigma \rangle$, and (c) the thermodynamic uncertainty $\mathcal{Q} = \text{nsr}\langle \Sigma \rangle / k_B$ as functions of β for $n = 25$ and $n = 50$. The values of $\hbar$, k_B, and ω are all set to 1.

Our findings demonstrate that by utilizing effects stemming from the collective system-bath coupling, the QIE can achieve a quadratic advantage in the mean work output, as compared to its independent counterpart in the large temperature limit. Additionally, we have shown that this collective advantage is present in other performance metrics as well, such as a low noise-to-signal ratio and low thermodynamic uncertainty, for appropriate parameter values. However, we emphasize that these collective advantages are limited to high temperatures only ($n\beta \ll 2/\hbar\omega$). In contrast, low temperatures favor independent operation of the setup, both in terms of the mean work output (see Fig. 2), as well as in terms of the thermodynamic uncertainty [see Fig. 6(c)]. Our research is motivated by recent findings that demonstrate that such collective effects can significantly enhance the performance of quantum heat engines [30–32,34,36]. However, in contrast to collective quantum heat engines, where the improvement in performance follows from collective enhancement in the specific heat of the WM, here the collective advantage stems from the higher occupation probabilities of the high positive magnetization states of the WM.

The quantum information engine proposed here can be expected to be experimentally realizable using already existing platforms. The details of the experimental protocols will depend on the details of the particular setups used. However, we note that a collective system-bath interaction, proposed in stroke 1, has been achieved using Rydberg atoms placed in a cavity [56], atomic sodium [57], quantum dots [58], and organic microcavities [59]. Independent system-bath coupling may be experimentally realized using nuclear spins in the presence of radio-frequency fields [60]. The measurement required in stroke 2 may be implemented by quantum magnetometers based on nitrogen-vacancy centers in diamond, which have been shown to be suitable for performing high-precision magnetometry [61–63]. Finally, the unitary U_{flip} in stroke 3 may be realized by applying a magnetic field aligned along the x axis [64]. The isolation of the WM from the bath during the strokes 2 and 3 can be achieved by ensuring that both the measurement process and the unitary operation occur rapidly compared to the thermalization time of the WM [65].

APPENDIX: FINITE-TEMPERATURE WORK AND ITS VARIANCE

The work outputs and their variances for the independent and collective engines can be calculated from Eqs. (5) and (6), as shown below for even and odd numbers of qubits,

$$\langle W_{\text{ind}}^{\text{even } n}\rangle = n\hbar\omega\left[\frac{2^n\Gamma\left(\frac{n+1}{2}\right)e^{\frac{1}{2}\beta(n+2)\hbar\omega}\,_2F_1\left(\frac{n}{2}, n+1, \frac{n}{2}+2, -e^{\beta\hbar\omega}\right)}{\sqrt{\pi}(e^{\beta\hbar\omega}+1)\Gamma\left(\frac{n}{2}+2\right)} - \tanh\frac{\beta\hbar\omega}{2}\right], \tag{A1}$$

$$\langle W_{\text{ind}}^{\text{odd } n}\rangle = \frac{2^n\hbar\omega\Gamma\left(\frac{n}{2}+1\right)e^{\frac{1}{2}\beta(n+1)\hbar\omega}\left[2\,_2F_1\left(2, \frac{1-n}{2}, \frac{n+3}{2}, -e^{\beta\hbar\omega}\right) - \,_2F_1\left(1, \frac{1-n}{2}, \frac{n+3}{2}, -e^{\beta\hbar\omega}\right)\right]}{\sqrt{\pi}\Gamma\left(\frac{n+3}{2}\right)(e^{\beta\hbar\omega}+1)^n} - n\hbar\omega\tanh\frac{\beta\hbar\omega}{2}, \tag{A2}$$

$$\langle W_{\text{col}}^{\text{even } n}\rangle = \frac{\hbar\omega\left[2e^{\frac{1}{2}\beta(n+2)\hbar\omega} - (n+2)e^{\beta\hbar\omega} + n\right]}{(e^{\beta\hbar\omega}-1)(e^{\beta(n+1)\hbar\omega}-1)}, \tag{A3}$$

$$\langle W_{\text{col}}^{\text{odd } n}\rangle = \frac{\hbar\omega\left[e^{\frac{1}{2}\beta(n+1)\hbar\omega} + e^{\frac{1}{2}\beta(n+3)\hbar\omega} - (n+2)e^{\beta\hbar\omega} + n\right]}{(e^{\beta\hbar\omega}-1)(e^{\beta(n+1)\hbar\omega}-1)}, \tag{A4}$$

$$\text{var}(W)_{\text{ind}}^{\text{even } n} = \frac{1}{4}\hbar^2\omega^2\,\text{sech}^2\frac{\beta\hbar\omega}{2}\left\{4n + \frac{2\Gamma(n+1)e^{\frac{\beta n\hbar\omega}{2}}}{\Gamma\left(\frac{n}{2}+2\right)\Gamma\left(\frac{n}{2}\right)}\,_2F_1\left(\frac{n}{2}, n+1, \frac{n}{2}+2, -e^{\beta\hbar\omega}\right)\right.$$
$$\times\left[-\frac{2^n n\Gamma\left(\frac{n+1}{2}\right)e^{\frac{1}{2}\beta(n+2)\hbar\omega}\,_2F_1\left(\frac{n}{2}, n+1, \frac{n}{2}+2, -e^{\beta\hbar\omega}\right)}{\sqrt{\pi}\Gamma\left(\frac{n}{2}+2\right)} + n(e^{\beta\hbar\omega}-1) - 2\right]$$
$$\left.-\frac{2n\Gamma(n+1)e^{\frac{\beta n\hbar\omega}{2}}}{\Gamma\left(\frac{n}{2}+2\right)\Gamma\left(\frac{n}{2}\right)}(e^{\beta\hbar\omega}+1)^{1-n}\,_2F_1\left(1, 1-\frac{n}{2}, \frac{n}{2}+2, -e^{\beta\hbar\omega}\right)\right\}, \tag{A5}$$

$$\text{var}(W)_{\text{col}}^{\text{even } n} = \frac{\hbar^2\omega^2 e^{\beta\hbar\omega}}{(e^{\beta\hbar\omega}-1)^2(e^{\beta(n+1)\hbar\omega}-1)^2}\left\{-n^2e^{\beta n\hbar\omega} + 4e^{\beta\hbar\omega+\frac{3\beta n\hbar\omega}{2}} + 4e^{\frac{1}{2}\beta(3n+4)\hbar\omega} - (n+2)^2e^{\beta(n+2)\hbar\omega}d\right.$$
$$\left.-4(n+1)e^{\frac{\beta n\hbar\omega}{2}} + 4(n+1)e^{\frac{1}{2}\beta(n+2)\hbar\omega} + 2(n(n+2)-4)e^{\beta(n+1)\hbar\omega} + 4\right\}, \tag{A6}$$

$$\text{var}(W)_{\text{ind}}^{\text{odd } n} = \frac{\hbar^2 \omega^2}{\pi (e^{\beta\hbar\omega} + 1)^2} \left\{ 4\pi n e^{\beta\hbar\omega} - \frac{(e^{\beta\hbar\omega} + 1)^{-2n}}{2\Gamma(\frac{n+3}{2})^2} \left\{ 2^{2n+1} \Gamma\left(\frac{n}{2} + 1\right)^2 e^{\beta(n+1)\hbar\omega} \right. \right.$$

$$\left. \times \left[n(e^{\beta\hbar\omega} - 1)\,_2F_1\left(1, \frac{1-n}{2}, \frac{n+3}{2}, -e^{\beta\hbar\omega}\right) + n + 1 \right]^2 + \pi(n+1)\Gamma(n+1)e^{\frac{1}{2}\beta(n+1)\hbar\omega}(e^{\beta\hbar\omega}+1)^n \right.$$

$$\left. \left. \times \left[-2ne^{\beta\hbar\omega}(n\cosh\beta\hbar\omega - n - 2)\,_2F_1\left(1, \frac{1-n}{2}, \frac{n+3}{2}, -e^{\beta\hbar\omega}\right) - (n+1)^2(e^{\beta\hbar\omega}-1) \right] \right\} \right\}, \quad (A7)$$

and

$$\text{var}(W)_{\text{col}}^{\text{odd } n} = \frac{\hbar^2\omega^2 e^{\frac{\beta\hbar\omega}{2}}}{(e^{\beta\hbar\omega}-1)^2(e^{\beta(n+1)\hbar\omega}-1)^2} \left\{ 4e^{\frac{\beta\hbar\omega}{2}} - (n^2+1)e^{\frac{\beta\hbar\omega}{2}+\beta n\hbar\omega} + 2(n-1)(n+3)e^{\frac{3\beta\hbar\omega}{2}+\beta n\hbar\omega} \right.$$

$$+ e^{\beta\hbar\omega + \frac{3\beta n\hbar\omega}{2}} - 2e^{\frac{1}{2}\beta(n+2)\omega} + e^{\frac{3}{2}\beta(n+2)\omega} + 6e^{\frac{1}{2}\beta(3n+4)\hbar\omega} - (2n+1)e^{\frac{\beta n\hbar\omega}{2}}$$

$$\left. + (2n+3)e^{\frac{1}{2}\beta(n+4)\hbar\omega} - [n(n+4)+5]e^{\frac{5\beta\hbar\omega}{2}+\beta n\hbar\omega} \right\}, \quad (A8)$$

where Γ represents the gamma function, and $_pF_q(a; b; z)$ denotes the hypergeometric function, which is defined as

$$_pF_q(a; b; z) \equiv {}_pF_q(a_1, \dots, a_p; b_1, \dots, b_q; z)$$

$$= \sum_{k=0}^{\infty} \frac{(a_1)_k \cdots (a_p)_k}{(b_1)_k \cdots (b_q)_k} \frac{z^k}{k!}. \quad (A9)$$

Here, the rising factorial $(x)_n$ is given by $(x)_n = x(x+1)(x+2)\cdots(x+n-1)$, $n \geq 1$.

The above finite-temperature equations can be simplified further by assuming the large n limit where the summation in Eqs. (5) and (6) can be replaced by integration, and we get Eq. (14) [see also Fig. 5(a)]. As expected, Eq. (14) simplifies to $\langle W_{\text{col}} \rangle \approx n\hbar\omega/4$ in the limit of $\beta \to 0$ (see Sec. III A). The variance of the output work can be obtained using Eq. (6), where the expression for the average of the square of the work in the large n limit takes the form

$$\langle W_{\text{col}}^2 \rangle = \frac{e^{\beta\hbar\omega r_{\max}}B - A}{\beta^2(e^a - 1)},$$

$A = [a(a+4)+8]$, $B = [b(b+4)+8]$, $a = \beta n\hbar\omega$, and $b = \beta\hbar\omega(n - 2r_{\max})$.

The mean work output $\langle W_{\text{ind}} \rangle$ is shown as a function of n for finite β in Fig. 7. $\langle W_{\text{ind}} \rangle$ increases with n until $n_{\text{opt}} \sim (k_B T/\hbar\omega)^2$, beyond which it decreases with increasing n [see Sec. III B and Fig. 5(a)].
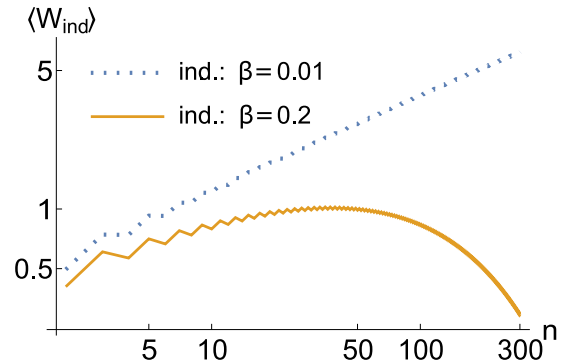

FIG. 7. The graph illustrates the mean work output of the independent engine at finite temperatures, for $\beta = 0.01$ and $\beta = 0.2$. The values of $\hbar$, k_B, and ω are set to 1. The plots clearly indicate a decrease in finite-temperature work output for higher n values, agreeing with the discussion in Sec. III B.

[1] S. Vinjanampathy and J. Anders, Quantum thermodynamics, Contemp. Phys. **57**, 545 (2016).

[2] S. W. Kim, T. Sagawa, S. De Liberato, and M. Ueda, Quantum Szilard engine, Phys. Rev. Lett. **106**, 070401 (2011).

[3] J. M. Diaz de la Cruz and M. A. Martin-Delgado, Quantum-information engines with many-body states attaining optimal extractable work with quantum control, Phys. Rev. A **89**, 032327 (2014).

[4] A. Aydin, A. Sisman, and R. Kosloff, Landauer's principle in a quantum Szilard engine without Maxwell's demon, Entropy **22**, 294 (2020).

[5] C. G. Knott, *Life and Scientific Work of Peter Guthrie Tait* (Cambridge University Press, Cambridge, UK, 1911), Vol. 1.

[6] E. Lutz and S. Ciliberto, From Maxwell's demon to Landauer's eraser, Phys. Today **68**(9), 30 (2015).

[7] É. Jussiau, L. Bresque, A. Auffèves, K. W. Murch, and A. N. Jordan, Many-body quantum vacuum fluctuation engines, Phys. Rev. Res. **5**, 033122 (2023).

[8] L. del Rio, J. Åberg, R. Renner, O. Dahlsten, and V. Vedral, The thermodynamic meaning of negative entropy, Nature (London) **474**, 61 (2011).

[9] N. M. Myers, O. Abah, and S. Deffner, Quantum thermodynamic devices: From theoretical proposals to experimental reality, AVS Quantum Sci. **4**, 027101 (2022).

[10] K. Yanik, B. Bhandari, S. K. Manikandan, and A. N. Jordan, Thermodynamics of quantum measurement and

Maxwell's demon's arrow of time, Phys. Rev. A **106**, 042221 (2022).

[11] C. Elouard, D. Herrera-Martí, B. Huard, and A. Auffeves, Extracting work from quantum measurement in Maxwell's demon engines, Phys. Rev. Lett. **118**, 260603 (2017).

[12] B. Bhandari and A. N. Jordan, Continuous measurement boosted adiabatic quantum thermal machines, Phys. Rev. Res. **4**, 033103 (2022).

[13] P. Kammerlander and J. Anders, Coherence and measurement in quantum thermodynamics, Sci. Rep. **6**, 22174 (2016).

[14] A. N. Jordan, C. Elouard, and A. Auffèves, Quantum measurement engines and their relevance for quantum interpretations, Quantum Stud.: Math. Found. **7**, 203 (2020).

[15] L. Bresque, P. A. Camati, S. Rogers, K. Murch, A. N. Jordan, and A. Auffèves, Two-qubit engine fueled by entanglement and local measurements, Phys. Rev. Lett. **126**, 120605 (2021).

[16] S. K. Manikandan, C. Elouard, K. W. Murch, A. Auffèves, and A. N. Jordan, Efficiently fueling a quantum engine with incompatible measurements, Phys. Rev. E **105**, 044137 (2022).

[17] L. Buffoni, A. Solfanelli, P. Verrucchi, A. Cuccoli, and M. Campisi, Quantum measurement cooling, Phys. Rev. Lett. **122**, 070603 (2019).

[18] J. V. Koski, V. F. Maisi, J. P. Pekola, and D. V. Averin, Experimental realization of a Szilard engine with a single electron, Proc. Natl. Acad. Sci. USA **111**, 13786 (2014).

[19] K. Wang, R. Xia, L. Bresque, and P. Xue, Experimental demonstration of a quantum engine driven by entanglement and local measurements, Phys. Rev. Res. **4**, L032042 (2022).

[20] D. Gelbwaser-Klimovsky, W. Niedenzu, and G. Kurizki, Thermodynamics of quantum systems under dynamical control, in *Advances in Atomic, Molecular, and Optical Physics*, edited by E. Arimondo, C. C. Lin, and S. F. Yelin (Academic Press, Cambridge, MA, 2015), Vol. 64, Chap. 12, pp. 329–407.

[21] S. Bhattacharjee and A. Dutta, Quantum thermal machines and batteries, Eur. Phys. J. B **94**, 239 (2021).

[22] C. L. Maria, B. Chitrak, and L. Amikam, Quantum engines and refrigerators, arXiv:2302.00726.

[23] V. Mukherjee and U. Divakaran, Many-body quantum thermal machines, J. Phys.: Condens. Matter **33**, 454001 (2021).

[24] R. Uzdin, A. Levy, and R. Kosloff, Equivalence of quantum heat machines, and quantum-thermodynamic signatures, Phys. Rev. X **5**, 031044 (2015).

[25] J. Roßnagel, O. Abah, F. Schmidt-Kaler, K. Singer, and E. Lutz, Nanoscale heat engine beyond the Carnot limit, Phys. Rev. Lett. **112**, 030602 (2014).

[26] W. Niedenzu, V. Mukherjee, A. Ghosh, A. G. Kofman, and G. Kurizki, Quantum engine efficiency bound beyond the second law of thermodynamics, Nat. Commun. **9**, 165 (2018).

[27] J. Klaers, S. Faelt, A. Imamoglu, and E. Togan, Squeezed thermal reservoirs as a resource for a nanomechanical engine beyond the Carnot limit, Phys. Rev. X **7**, 031044 (2017).

[28] O. Abah, G. De Chiara, M. Paternostro, and R. Puebla, Harnessing nonadiabatic excitations promoted by a quantum critical point: Quantum battery and spin squeezing, Phys. Rev. Res. **4**, L022017 (2022).

[29] R. Alicki and M. Fannes, Entanglement boost for extractable work from ensembles of quantum batteries, Phys. Rev. E **87**, 042123 (2013).

[30] W. Niedenzu and G. Kurizki, Cooperative many-body enhancement of quantum thermal machine power, New J. Phys. **20**, 113038 (2018).

[31] M. Kloc, P. Cejnar, and G. Schaller, Collective performance of a finite-time quantum Otto cycle, Phys. Rev. E **100**, 042126 (2019).

[32] C. L. Latune, I. Sinayskiy, and F. Petruccione, Collective heat capacity for quantum thermometry and quantum engine enhancements, New J. Phys. **22**, 083049 (2020).

[33] L. da Silva Souza, G. Manzano, R. Fazio, and F. Iemini, Collective effects on the performance and stability of quantum heat engines, Phys. Rev. E **106**, 014143 (2022).

[34] N. Jaseem, S. Vinjanampathy, and V. Mukherjee, Quadratic enhancement in the reliability of collective quantum engines, Phys. Rev. A **107**, L040202 (2023).

[35] D. Kolisnyk and G. Schaller, Performance boost of a collective qutrit refrigerator, Phys. Rev. Appl. **19**, 034023 (2023).

[36] D. Gelbwaser-Klimovsky, W. Kopylov, and G. Schaller, Cooperative efficiency boost for quantum heat engines, Phys. Rev. A **99**, 022129 (2019).

[37] F. Campaioli, F. A. Pollock, and S. Vinjanampathy, *Quantum Batteries* (Springer, Cham, 2018), pp. 207–225.

[38] C. L. Latune, I. Sinayskiy, and F. Petruccione, Thermodynamics from indistinguishability: Mitigating and amplifying the effects of the bath, Phys. Rev. Res. **1**, 033192 (2019).

[39] H. P. Breuer and F. Petruccione, *The Theory of Open Quantum Systems* (Oxford University Press, Oxford, UK, 2002).

[40] L. Mandel and E. Wolf, *Optical Coherence and Quantum Optics* (Cambridge University Press, Cambridge, UK, 1995).

[41] T. Koshy, *Catalan Numbers with Applications* (Oxford University Press, Oxford, UK, 2008).

[42] R. P. Stanley, *Catalan Numbers* (Cambridge University Press, Cambridge, UK, 2015).

[43] M. F. Sacchi, Thermodynamic uncertainty relations for bosonic Otto engines, Phys. Rev. E **103**, 012111 (2021).

[44] A. C. Barato and U. Seifert, Thermodynamic uncertainty relation for biomolecular processes, Phys. Rev. Lett. **114**, 158101 (2015).

[45] P. Pietzonka and U. Seifert, Universal trade-off between power, efficiency, and constancy in steady-state heat engines, Phys. Rev. Lett. **120**, 190602 (2018).

[46] J. M. Horowitz and T. R. Gingrich, Thermodynamic uncertainty relations constrain non-equilibrium fluctuations, Nat. Phys. **16**, 15 (2020).

[47] G. Guarnieri, G. T. Landi, S. R. Clark, and J. Goold, Thermodynamics of precision in quantum nonequilibrium steady states, Phys. Rev. Res. **1**, 033021 (2019).

[48] P. Menczel, E. Loisa, K. Brandner, and C. Flindt, Thermodynamic uncertainty relations for coherently driven open quantum systems, J. Phys. A: Math. Theor. **54**, 314002 (2021).

[49] A. Das, S. Mahunta, B. K. Agarwalla, and V. Mukherjee, Precision bound in periodically modulated continuous quantum thermal machines, Phys. Rev. E **108**, 014137 (2023).

[50] B. K. Agarwalla and D. Segal, Assessing the validity of the thermodynamic uncertainty relation in quantum systems, Phys. Rev. B **98**, 155438 (2018).

[51] K. Ptaszyński, Coherence-enhanced constancy of a quantum thermoelectric generator, Phys. Rev. B **98**, 085425 (2018).

[52] L. M. Cangemi, V. Cataudella, G. Benenti, M. Sassetti, and G. De Filippis, Violation of thermodynamics uncertainty relations in a periodically driven work-to-work converter from weak to strong dissipation, Phys. Rev. B **102**, 165418 (2020).

[53] A. A. Sand Kalaee, A. Wacker, and P. P. Potts, Violating the thermodynamic uncertainty relation in the three-level maser, Phys. Rev. E **104**, L012103 (2021).

[54] M. F. Sacchi, Multilevel quantum thermodynamic swap engines, Phys. Rev. A **104**, 012217 (2021).

[55] P. P. Potts and P. Samuelsson, Thermodynamic uncertainty relations including measurement and feedback, Phys. Rev. E **100**, 052137 (2019).

[56] J. M. Raimond, P. Goy, M. Gross, C. Fabre, and S. Haroche, Collective absorption of blackbody radiation by Rydberg atoms in a cavity: An experiment on Bose statistics and Brownian motion, Phys. Rev. Lett. **49**, 117 (1982).

[57] M. Gross, C. Fabre, P. Pillet, and S. Haroche, Observation of near-infrared Dicke superradiance on cascading transitions in atomic sodium, Phys. Rev. Lett. **36**, 1035 (1976).

[58] M. Scheibner, T. Schmidt, L. Worschech, A. Forchel, G. Bacher, T. Passow, and D. Hommel, Superradiance of quantum dots, Nat. Phys. **3**, 106 (2007).

[59] J. Q. Quach, K. E. McGhee, L. Ganzer, D. M. Rouse, B. W. Lovett, E. M. Gauger, J. Keeling, G. Cerullo, D. G. Lidzey, and

[60] T. Virgili, Superabsorption in an organic microcavity: Toward a quantum battery, Sci. Adv. **8**, eabk3160 (2022).

[60] J. P. S. Peterson, T. B. Batalhão, M. Herrera, A. M. Souza, R. S. Sarthour, I. S. Oliveira, and R. M. Serra, Experimental characterization of a spin quantum heat engine, Phys. Rev. Lett. **123**, 240601 (2019).

[61] H. J. Mamin, M. H. Sherwood, M. Kim, C. T. Rettner, K. Ohno, D. D. Awschalom, and D. Rugar, Multipulse double-quantum magnetometry with near-surface nitrogen-vacancy centers, Phys. Rev. Lett. **113**, 030803 (2014).

[62] G. Balasubramanian, I. Y. Chan, R. Kolesov, M. Al-Hmoud, J. Tisler, C. Shin, C. Kim, A. Wojcik, P. R. Hemmer, A. Krueger *et al.*, Nanoscale imaging magnetometry with diamond spins under ambient conditions, Nature (London) **455**, 648 (2008).

[63] Y. Wu and T. Weil, Recent developments of nanodiamond quantum sensors for biological applications, Adv. Sci. **9**, 2200059 (2022).

[64] S. Bodenstedt, I. Jakobi, J. Michl, I. Gerhardt, P. Neumann, and J. Wrachtrup, Nanoscale Spin manipulation with pulsed magnetic gradient fields from a hard disc drive writer, Nano Lett. **18**, 5389 (2018).

[65] H.-P. Breuer and F. Petruccione, *The Theory of Open Quantum Systems* (Oxford University Press, New York, 2002).